Thermal flexure and glacier calving

Bradley Paul Lipovsky

Dept. of Earth and Planetary Sciences, Harvard University

Key Points:

- Thermal flexure is a type of glacier–ocean interaction that has not previously been described.
- Thermal flexure influences both rotational (i.e., Greenland-style) and tabular (i.e., Antarctic-style) iceberg calving.
- Thermal flexure may cause either top-out or bottom-out ice front rotation depending on the ice thermal state.

Corresponding author: Bradley Paul Lipovsky, brad_lipovsky@fas.harvard.edu

Abstract

Glaciers and ice sheets that terminate in bodies of water are expected to undergo thermal expansion as ice comes into contact with much warmer liquid water. Here, I investigate the roll that this thermal expansion plays in the fracturing processes that give rise to glacier calving. I find that thermal expansion may cause either top-out or bottom-out rotation of a partially submerged ice cliff. I analyze temperature borhole data from Greenland and Antarctica and find that ice cliff thermal flexure exceeds the flexure due to buoyancy forces. This flexure may plausibly account for the some of the net torque that gives rise to rotational calving events in Greenland. Thermal expansion in ice shelves, in contrast, may either stabilize or destabilize rift propagation depending on the ice shelf thermal environment. This study highlights the previously unexplored role of thermal fracture in the stability of glaciers and ice sheets.

1 Introduction

Calving, defined as the separation of ice blocks from a glacier's margin, is a basic component of glacier force and mass balance (Cuffey & Paterson, 2010). Calving is a fracturing process that occurs upon connection of one or multiple fractures. Benn et al. (2007) summarize the forces that are thought to drive these fractures. They are: longitudinal stresses due to stretching, a net force exerted on the glacier margin, a net moment exerted on the glacier margin, and cliff undercutting. Here, I investigate the role of a another process that may act to drive or suppress calving: thermal expansion of ice in contact with much warmer ocean or lake water.

All materials experience thermal expansion and contraction as they are heated or cooled relative to a reference state (Petrenko & Whitworth, 1999). Indeed, thermal fracture in ice has been previously studied in sea ice (Bažant, 1992), for generic floating ice plates (Evans & Untersteiner, 1971), and in laboratory experiments (Gold, 1963). Goldstein & Osipenko (2006) carried out an analysis of thermal fracture in ice using linear elastic fracture mechanics (LEFM). More recently, several studies have found surficial glacier and ice sheet seismicity associated with fracturing and cold air temperatures (Podolskiy et al., 2018; MacAyeal et al., 2018; Olinger et al., 2019). To my knowledge, no previous study has sought to explicitly relate thermal fracture to glacier calving.

2 Observations

I consider four different temperature profiles as plotted in Figure 1a. Three of these profiles are from Antarctic ice shelves, including the Ross Little America V site (Bender et al., 1961), the Ross J9 site (Clough & Hansen, 1979), and the Pine Island Ice Shelf Site A (Stanton et al., 2013). At Pine Island Site A, temperatures were only collected in the lowermost 112 m by Stanton et al. (2013) and in the uppermost 10 m by Mulvaney & Smith (2017). I assume that the Pine Island Site A has a vertically uniform profile in the depth range where no measurements are available. This assumption is informed by modeling efforts which support the existence of a uniform temperature profile with depth in ice shelves with significant basal melting (Sergienko et al., 2013).

Few borehole data are available near marine terminating outlet glaciers in Greenland. To my knowledge, the only such borehole data are those reported at Jakobshavn Isbrae by Iken et al. (1993) and at a nearby site by Lüthi et al. (2002). These data were recorded in grounded ice about 50 km upstream from the calving front. The Jakobshavn profile has warm temperatures in the uppermost part of the column due to the latent heat transferred during the refreezing of surface meltwater (Echelmeyer et al., 1992). Similar features are observed in the land-terminating part of the Greenland Ice Sheet (Harrington et al., 2015). These boreholes reached at most 65% of the ice thickness and the

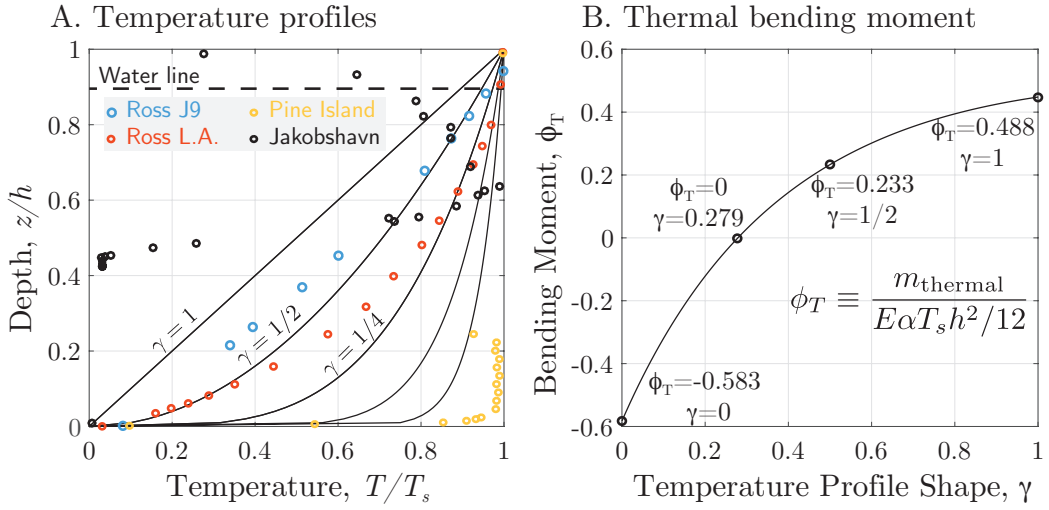

Figure 1. A. Comparaison of borehole temperatures with idealized temperature profiles and B. resulting thermal bending stresses. As noted in the text, the Pine Island data are combined from two different measurement epochs and the Jakobshavn profile is inferred to be temperate in the lower third of the profile.

ice below this thickness is therefore inferred to be at the pressure melting point (Funk et al., 1994).

This wide range of observed temperature profiles motivates an examination of the role that thermal structure plays in generating thermal stresses during calving.

3 Model of thermal bending

Thermal expansion is expected to occur along ice cliffs that suddenly come into contact with water. To model this phenomenon, I treat ice as a thermo-elastic material. I neglect viscous flow and therefore limit attention to time periods shorter than the Maxwell viscoelastic relaxation timescale, i.e. on the order of hours to weeks depending on the ice strain rate (MacAyeal & Sergienko, 2013; Lipovsky & Dunham, 2017). This analysis is therefore relevant to calving processes including rapid ice shelf rift propagation (e.g., Banwell et al., 2017) and quickly repeating tidewater calving events (e.g., James et al., 2014).

3.1 Buoyancy-driven flexure

I begin by recalling the details of the buoyancy forces that act on a partially submerged ice cliff (Weertman, 1957; Reeh, 1968) with the goal of providing context for thermal loading. I consider a generic floating ice cliff that may represent a face of an iceberg, an ice shelf rift wall, an ice shelf calving front, or a calving glacier ice front. Buoyancy loading results from two contributions: the overburden stress in the ice and the water pressure acting on the ice. The net extensional or membrane stress due to the hydrostatic ocean load and the ice overburden is,

$$\sigma_0 \equiv \frac{\rho g h}{2}\left(1 - \frac{h_w}{h}\right), \tag{1}$$

where ρ is the density of ice, g is the acceleration due to gravity, h is the ice thickness, $h_w/h = \rho/\rho_w$ is the submerged fraction of the ice thickness assuming flotation, and ρ_w

is the density of water. Similarly, the combined moment due to the hydrostatic ocean load and the ice overburden is,

$$m_0 \equiv \frac{\rho_w g h^3}{12}\left[3\left(\frac{h_w}{h}\right)^2 - 2\left(\frac{h_w}{h}\right)^3 - \left(\frac{h_w}{h}\right)\right] \equiv \phi_0 \frac{\rho_w g h^3}{12} \tag{2}$$

For $\rho/\rho_w = 0.90$, $\phi_0 = 0.072$. For values of ρ/ρ_w relevant to ice floating in water, ϕ_0, $m_0 > 0$, corresponding to top-out rotation. I will often express bending moments as equivalent bending stresses at the top of the ice shelf, $\sigma_b \equiv 6m/h^2$.

3.2 Thermal flexure

I consider a temperature difference $\Delta T(z)$ between the ice and the water creates thermal strain $\alpha \Delta T(z)$, where $\alpha = 5 \times 10^{-5}$ °C^{-1} is the coefficient of thermal expansion of ice (Petrenko & Whitworth, 1999). The bending moment associated with this thermal expansion is (Bažant, 1992, Equation 4),

$$m_{thermal} \equiv \frac{E'\alpha}{h}\int_0^{h_w} (z - h/2)\Delta T(z)\, dz, \tag{3}$$

where $E' \equiv E/(1-\nu)$, and $E = 9$ GPa and $\nu = 0.3$ are Young's modulus and Poisson's ratio of ice, respectively.

Thermal expansion acts to create depth varying thermal strains that can be approximated as the sum of a depth-averaged thermal strain plus depth-varying thermal flexure. Importantly, depth-averaged thermal strains will only induce mechanical stresses if confinement is present (Eslami et al., 2013). If, for example thermal expansion causes the walls of an ice shelf rift to come into contact and press against each other, this action will create a state of compression along the rift walls. If, on the other hand, thermal expansion occurs along an unconfined ice front, a bending moment may be generated yet no stress changes will occur.

With this caveat in mind, I calculate the depth-averaged thermal stress,

$$\sigma_{thermal} \equiv \frac{E'\alpha}{h}\int_0^{h_w} \Delta T(z)\, dz. \tag{4}$$

This stress is equal and opposite in sign to the stress required to create a state of zero net extensional strain (Eslami et al., 2013).

3.3 Thermal profiles

I consider a range of simplified temperature profiles that reflect two end-member situations: a steady state linear temperature profile and a vertical-constant temperature profile dominated by downward advection and basal melting (Sergienko et al., 2013). These two end-member cases may be approximately modeled using a simple polynomial temperature profile with coldest ice at the surface and warmest ice at the bed,

$$\Delta T(z) = T_s \left(\frac{z}{h}\right)^{\gamma}. \tag{5}$$

With this notation, $-T_s$ is the ice surface temperature in degrees Celcius; with this sign convention ΔT is positive. The exponent γ accounts for the shape of the temperature profile. Values of γ near unity reflect a linear temperature profile as is typical of an ice column with net basal accumulation, whereas values of γ near zero reflect a nearly constant temperature profile typical of an ice column with extreme basal melting (Sergienko et al., 2013). These two cases, and the resulting thermal bending stresses are plotted in Figure 1.

For the temperature profile of Equation 5, the thermal bending moment is,

$$\begin{aligned} m_{thermal} &\equiv E'\alpha T_s h^2 \int_0^{h_w/h} \left(\frac{z}{h}\right)^{\gamma} \left(\frac{z}{h} - \frac{1}{2}\right)\, d(z/h) \\ &= E'\alpha T_s h^2 \left(\frac{h_w}{h}\right)^{\gamma+1} \left[\frac{1}{\gamma+2}\left(\frac{h_w}{h}\right) - \frac{1}{2(\gamma+1)}\right] \\ &\equiv \phi_T \frac{E'\alpha T_s h^2}{12}. \end{aligned} \tag{6}$$

Similarly, the maximum confined thermal stress is

$$\sigma_{thermal} = E'\alpha \frac{T_s}{h} \int_0^{h_w} \left(\frac{z}{h}\right)^{\gamma}\, dz = \frac{E'\alpha T_s}{\gamma+1} \left(\frac{h_w}{h}\right)^{\gamma+1}. \tag{7}$$

The thermal bending moment changes sign as a function of curvature of the temperature profile. This phenomenon is shown schematically in Figure 2. This changes occurs within the function $\phi_T(\gamma)$, as shown in Figure 1. Ice columns with nearly uniform temperature profiles (e.g., one dominated by downward thermal advection) experience bottom-out rotation, whereas ice columns with linear temperature profiles (e.g., an ice shelf with basal accretion) experience top-out rotation. I next apply this model to observed temperature profiles.

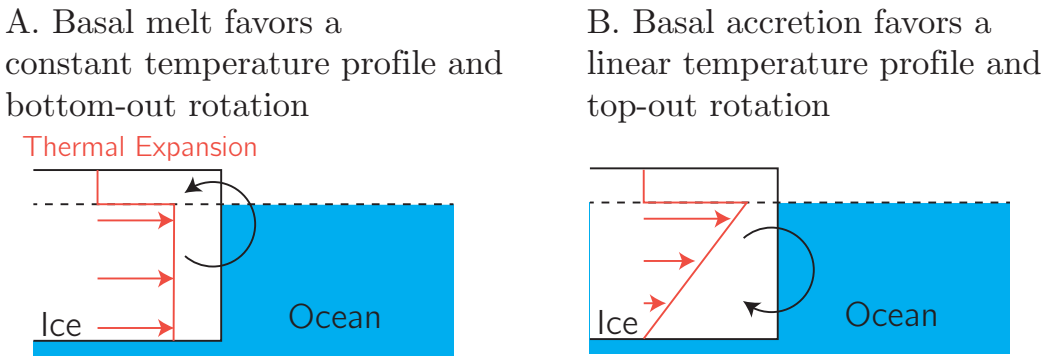

Figure 2. Thermal expansion along an ice front may result in either (A.)bottom-out or (B.) top-out rotation depending on the shape of the ice shelf vertical temperature profile. Top-out rotation puts the bottom half of the ice shelf in tension and therefore reduces the stabilizing effect of deep, ductile ice.

4 Results

For ice shelf sites, I calculate buoyancy stresses (Equation 1), buoyancy moments (Equation 2), thermal moments (Equation 6), and thermal stresses (Equation 7). The results are given in Table 2. At all ice shelf sites the thermal bending moments exceed the buoyancy bending moments. For the J9, Little America, and Pine Island sites, $m_T/m_0 = 6$, 30, and 23, respectively. Depth averaged thermal stresses are also greater than depth averaged buoyancy stresses by factors of 6, 10, and 7, respectively.

For the Jakobshavn data, I calculate thermal stresses and moments using Equations 4 and 3, respectively. Thermal bending moments at Jakobshavn are calculated to be the largest of any temperature profile considered here (Table 2). These large moments

Table 1. Parameters used in calculations

	Thickness	Min. Temp.	Factor (ϕ_T)	Shape (γ)
Ross J9	420 m	-26.4°C	0.11	0.75
Ross Little America	254 m	-21.5°C	0.41	0.33
Pine Island A	460 m	-22.4°C	-0.54	0
Jakobshavn	833 m	-22.4°C	n/a	n/a

Table 2. Table of calculated stresses (MPa)

	Flexural		Depth-Averaged	
	Buoyancy	Thermal	Buoyancy	Thermal
Ross J9	0.15	0.93	1.7	-8.6
Ross Little America	0.093	2.8	1.0	-9.7
Pine Island A	0.17	-3.9	1.9	-13.9
Jakobshavn	0.30	5.7	3.4	-5.1

occur because of the localization of thermal expansion to the upper half of the ice column. The thermal moment is calculated to be 19 times larger than the buoyancy moment. The depth integrated thermal stress, in contrast, is only 1.5 times larger than the depth integrated buoyancy stress (Table 2).

5 Discussion

5.1 Ice shelf rift propagation

Ice shelf calving is dominated by the formation of tabular icebergs through the process of rift propagation (Benn et al., 2007). Rifts are defined as through-cutting fractures in ice shelves; as such, their propagation is defined to be in the horizontal plane (Hulbe et al., 2010), with the possible exception of a small process region near the rift tip (Lipovsky, 2018). Lipovsky (2019) recently conducted three-dimensional simulations of rift propagation under the assumptions of linear elastic fracture mechanics. This study describes the process of flexural stabilization whereby buoyancy-induced flexure of rift walls causes rift closure and thereby acts as stabilizing process during rift propagation. Rfit closure was found to occur at the top of the rift due to the top-out sense of rotation caused by buoyancy loading. This study found that flexural stabilization results in an effective fracture toughness K_I^b that scales proportionally with the total bending stress σ_b,

$$K_I^b \equiv -\sigma_b f(\nu)\sqrt{\lambda} \tag{8}$$

where the factor $f(\nu = 0.3) = 0.7646$ and the flexural wavelength is $\lambda^4 \equiv D/(\rho_w g)$ with flexural rigidity $D \equiv h^3 E/(1-\nu^2)/12$.

Thermal flexure may be treated by superposition in the linear model of Lipovsky (2019). Examining the sum of buoyancy and thermal bending in Table 2 shows that thermal flexure enhances flexural stability at the two Ross sites. At Pine Island, however, the net bending stress is negative suggesting that bottom-out rotation occurs. This sense of rotation has been observed on rapidly-melting icebergs by (Scambos et al., 2005). Bottom-out rotation of rift walls results in opening at the top of a rift and closure at the bottom. I hypothesize that this sense of motion is destabilizing because it provides a pathway for hydraulic fracture as water rushes in to the opened, upper part of the rift tip region. Together, these results suggest that basal melting may destabilize ice shelf rift

propagation. Basal freeze-on is expected to have the opposite effect. A full examination of this process would require three dimensional fracture simulations, however, and is therefore beyond the scope of the present work.

5.2 Calving at tidewater glaciers

Tidewater glacier calving in Greenland is dominated by the detachment of large (km-scale) blocks with narrow aspect ratio, i.e., blocks that are long in the cross-glacier direction but narrow in the along-flow direction (Benn et al., 2007). Recent studies show that these blocks detach when a vertically propagating basal crevasse reaches the surface (Murray et al., 2015). Several approaches have been used to model fracturing processes in this setting including a strength of materials approach (Wagner et al., 2016) and linear elastic fracture mechanics (Van der Veen, 1998; Jimenez & Duddu, 2018). Given the limited number of borehole temperature observations in this setting, however, I focus here just on flexural processes rather than on the fracturing processes.

At Helheim Glacier, James et al. (2014) observed a series of calving events that resulted in more than 1 km of front retreat over a 6 d period. These authors subsequently observed an uplift of the ice front equal to about $w_* = 20$ m. James et al. (2014) and Wagner et al. (2016) both suggest that this upward tilting at Helheim is caused by the glacier flowing into the fjord at a steep angle and then being driven to a depth below flotation. The upward tilt in this explanation results from the ice deforming upward towards buoyant equilibrium. James et al. (2014), however, point out a limitation to this explanation, namely, that upward tilt also occurs where ice becomes ungrounded with the opposite direction of bed slope.

The initial series of calving events observed by James et al. (2014) exposed cold interior ice to warm ocean waters and therefore plausibly resulted in ice front thermal expansion. To compare with observations, I solve the floating beam equation and find a relationship between the ice front uplift w_* and moment $m_* = -\rho_w g w_* \lambda^2/2$ (Hetényi, 1971). At Helheim the ice front thickness is ∼740 m giving $D = 3.3 \times 10^{17}$ Nm, $\lambda =$ 1.7 km, and $m_* = -290$ GN. Using Equation 6, I calculate that the observed uplift is accounted for with a vertically uniform temperature profile ($\gamma = 0$) with ice temperature $-22°$C.

6 Conclusions

Thermal expansion constitutes a previously undescribed type of ice–ocean interaction. Gradients in thermal expansion create a bending moment acting on an ice cliff that may cause either top-out or bottom-out rotation. I show that thermal bending moments may be larger than the bending moment created by buoyancy forces. Thermal flexure appears to play a role in the the fracturing process during both Greenlandic rotational calving and Antarctic ice shelf rift propagation. These results provide a new perspective on the precarious nature of glaciers and ice sheets that terminate in liquid water.

Acknowledgments

This manuscript benefited from early discussions with Douglas MacAyeal. The author was supported by the Department of Earth and Planetary Sciences at Harvard University. All data in this manuscript are previously published and cited appropriately.

References

Banwell, A. F., Willis, I. C., Macdonald, G. J., Goodsell, B., Mayer, D. P., Powell, A., & Macayeal, D. R. (2017). Calving and rifting on the McMurdo Ice Shelf,

Antarctica. *Annals of Glaciology*, 1–10.

Bažant, Z. P. (1992). Large-scale thermal bending fracture of sea ice plates. *Journal of Geophysical Research: Oceans*, *97*(C11), 17739–17751.

Bender, J., AJ, & Gow. (1961). Deep drilling in antarctica. In *Colloque sur la glaciologie antarctique* (pp. 132–141).

Benn, D. I., Warren, C. R., & Mottram, R. H. (2007). Calving processes and the dynamics of calving glaciers. *Earth-Science Reviews*, *82*(3), 143–179.

Clough, J. W., & Hansen, B. L. (1979). The ross ice shelf project. *Science*, *203*(4379), 433–434.

Cuffey, K. M., & Paterson, W. S. B. (2010). *The physics of glaciers*. Academic Press.

Echelmeyer, K., Harrison, W., Clarke, T., & Benson, C. (1992). Surficial glaciology of Jakobshavns Isbræ, west Greenland: Part II. Ablation, accumulation and temperature. *Journal of Glaciology*, *38*(128), 169–181.

Eslami, M. R., Hetnarski, R. B., Ignaczak, J., Noda, N., Sumi, N., & Tanigawa, Y. (2013). *Theory of elasticity and thermal stresses* (Vol. 197). Springer.

Evans, R., & Untersteiner, N. (1971). Thermal cracks in floating ice sheets. *Journal of Geophysical Research*, *76*(3), 694–703.

Funk, M., Echelmeyer, K., & Iken, A. (1994). Mechanisms of fast flow in jakobshavns isbræ, west greenland: Part ii. modeling of englacial temperatures. *Journal of Glaciology*, *40*(136), 569–585.

Gold, L. W. (1963). Crack formation in ice plates by thermal shock. *Canadian journal of physics*, *41*(10), 1712–1728.

Goldstein, R. V., & Osipenko, N. M. (2006). Fracture of ice cover under thermal stresses. *Geophysica*, *42*(1-2), 3–15.

Harrington, J. A., Humphrey, N. F., & Harper, J. T. (2015). Temperature distribution and thermal anomalies along a flowline of the greenland ice sheet. *Annals of Glaciology*, *56*(70), 98–104.

Hetényi, M. (1971). *Beams on elastic foundation: theory with applications in the fields of civil and mechanical engineering* (No. BOOK). University of Michigan.

Hulbe, C. L., LeDoux, C., & Cruikshank, K. (2010). Propagation of long fractures in the Ronne Ice Shelf, antarctica, investigated using a numerical model of fracture propagation. *Journal of Glaciology*, *56*(197), 459–472.

Iken, A., Echelmeyer, K., Harrison, W., & Funk, M. (1993). Mechanisms of fast flow in jakobshavns isbræ, west greenland: Part i. measurements of temperature and water level in deep boreholes. *Journal of Glaciology*, *39*(131), 15–25.

James, T. D., Murray, T., Selmes, N., Scharrer, K., & OLeary, M. (2014). Buoyant flexure and basal crevassing in dynamic mass loss at helheim glacier. *Nature Geoscience*, *7*(8), 593.

Jimenez, S., & Duddu, R. (2018). On the evaluation of the stress intensity factor in calving models using linear elastic fracture mechanics. *Journal of Glaciology*, *64*(247), 759–770.

Lipovsky, B. P. (2018). Ice shelf rift propagation and the mechanics of wave-induced fracture. *Journal of Geophysical Research: Oceans*.

Lipovsky, B. P. (2019). *Ice shelf rift propagation: stability, three dimensional effects, and the role of marginal weakening*. The Cryosphere Discuss. doi: 10.5194/tc-2019-232

Lipovsky, B. P., & Dunham, E. M. (2017). Slow-slip events on the Whillans Ice Plain, Antarctica, described using rate-and-state friction as an ice stream sliding law. *Journal of Geophysical Research: Earth Surface*, *122*(4), 973–1003.

Lüthi, M., Funk, M., Iken, A., Gogineni, S., & Truffer, M. (2002). Mechanisms of fast flow in jakobshavn isbræ, west greenland: Part iii. measurements of ice deformation, temperature and cross-borehole conductivity in boreholes to the bedrock. *Journal of Glaciology*, *48*(162), 369–385.

MacAyeal, D. R., Banwell, A. F., Okal, E. A., Lin, J., Willis, I. C., Goodsell, B., & MacDonald, G. J. (2018). Diurnal seismicity cycle linked to subsurface melting on an ice shelf. *Annals of Glaciology*, 1–21.

MacAyeal, D. R., & Sergienko, O. V. (2013). The flexural dynamics of melting ice shelves. *Annals of Glaciology*, *54*(63), 1–10.

Mulvaney, R., & Smith, A. (2017). *Pine Island Glacier mean annual temperatures - collected 2014-2015*. Polar Data Centre, Cambridge, UK. doi: doi:10.5285/eae547d0-9668-4ba1-9fc4-67929382395f

Murray, T., Nettles, M., Selmes, N., Cathles, L., Burton, J., James, T., ... others (2015). Reverse glacier motion during iceberg calving and the cause of glacial earthquakes. *Science*, aab0460.

Olinger, S., Lipovsky, B., Wiens, D., Aster, R., Bromirski, P., Chen, Z., ... Stephen, R. (2019). Tidal and thermal stresses drive seismicity along a major ross ice shelf rift. *Geophysical Research Letters*, *46*(12), 6644–6652.

Petrenko, V. F., & Whitworth, R. W. (1999). *Physics of ice*. OUP Oxford.

Podolskiy, E. A., Fujita, K., Sunako, S., Tsushima, A., & Kayastha, R. B. (2018). Nocturnal thermal fracturing of a himalayan debris-covered glacier revealed by ambient seismic noise. *Geophysical Research Letters*, *45*(18), 9699–9709.

Reeh, N. (1968). On the calving of ice from floating glaciers and ice shelves. *Journal of Glaciology*, *7*(50), 215–232.

Scambos, T., Sergienko, O., Sargent, A., MacAyeal, D., & Fastook, J. (2005). Icesat profiles of tabular iceberg margins and iceberg breakup at low latitudes. *Geophysical Research Letters*, *32*(23).

Sergienko, O., Goldberg, D., & Little, C. (2013). Alternative ice shelf equilibria determined by ocean environment. *Journal of Geophysical Research: Earth Surface*, *118*(2), 970–981.

Stanton, T., Shaw, W., Truffer, M., Corr, H., Peters, L., Riverman, K., ... Anandakrishnan, S. (2013). Channelized ice melting in the ocean boundary layer beneath pine island glacier, antarctica. *Science*, *341*(6151), 1236–1239.

Van der Veen, C. (1998). Fracture mechanics approach to penetration of surface crevasses on glaciers. *Cold Regions Science and Technology*, *27*(1), 31–47.

Wagner, T. J., James, T. D., Murray, T., & Vella, D. (2016). On the role of buoyant flexure in glacier calving. *Geophysical Research Letters*, *43*(1), 232–240A.

Weertman, J. (1957). Deformation of floating ice shelves. *Journal of glaciology*, *3*(21), 38–42.